JOURNAL OF AIRCRAFT
Vol. 43, No. 3, May–June 2006

Monitoring Global Positioning System Satellite Orbit Errors for Aircraft Landing Systems

Jiyun Lee,* Sam Pullen,† and Per Enge‡
Stanford University, Stanford, California 94305-4085
and
Boris Pervan§ and Livio Gratton¶
Illinois Institute of Technology, Chicago, Illinois 60616-3793

Ground-based augmentations of the global positioning system (GPS) demand the greatest safety and reliability to support aircraft precision approach and landing navigation. One troublesome failure mode for these systems is the possibility of large orbit errors; discrepancies between the locations of GPS satellites in space and the locations derived by the ephemeris data that they broadcast. To counter this possibility, several ephemeris monitor algorithms detecting orbit errors are described. The method is based on a comparison between satellite positions given by the current satellite ephemeris [today's ephemeris (TE)] and the ephemeris broadcast by the same satellite on its preceding pass [yesterday's ephemeris (YE)]. Variants of this YE–TE test are shown to provide protection against ephemeris errors and also to support minimum detectable errors as low as 1145 m, which will minimize the resulting impact on ground-based augmentation system user availability. In addition, to initialize these monitors when no earlier validated ephemerides are available, means of using raw measurements are proposed. The results show that the YE–TE and the measurement-based methods together are adequate to meet navigation integrity and availability requirements for category 1 precision approaches.

I. Introduction

THE use of differential global positioning system (DGPS) enhances stand-alone GPS accuracy such that it is sufficient for all phases of aviation navigation, including aircraft precision approaches and landings. However, improving accuracy with DGPS is not enough to support such difficult operations. The navigation system must also guarantee flight safety by providing warnings for any system failures or anomalies and assuring the position solution at a reliable level with protection bounds. Major applications of DGPS designed to fulfill these needs are ground-based augmentation systems (GBAS), such as the local area augmentation system (LAAS) being developed by the Federal Aviation Administration. In this work, detailed consideration is given to monitoring a specific source of navigation failure, incorrect knowledge of a GPS satellite orbit, that is, ephemeris errors, and providing ephemeris protection levels.

GPS users compute their position using ranging measurements obtained from the satellite signals and the satellite location derived by the broadcast ephemerides. Thus, an error in the knowledge of satellite orbits will result in an error in the computed user position. GBAS users can eliminate common-mode errors by applying differential corrections to their ranging measurements.[1] Under nominal conditions, GPS satellite ephemeris errors are so small (typically 10 m or less in three dimensions, with the along-track direction containing most of the error[2]) that the differential pseudorange error between GBAS reference receivers and users is negligible. However, this does not preclude the possibility that a failure will cause satellite ephemeris errors large enough to threaten GBAS users.

The differential corrections are derived from scalar ranges, and, thus, ephemeris errors orthogonal to the line of sight between a failed satellite and a GBAS ground station are not accounted for. Moreover, position errors caused by orbit errors are dependent on the time-varying displacement between the aircraft and GBAS reference receivers. If this harmful anomaly were to occur, the responsibility for detecting and excluding these failures would lie with the GBAS ground facility rather than with users. To the extent that the ground facility cannot do this, the user must be notified of the magnitude of the possible (undetectable) hazard so that his computed position protection levels include it.

To help validate adequate GBAS protection against ephemeris threats, two types of ephemeris failures, type A and type B, have been identified.[3] The first type is subdivided into two classes: type A1 and type A2. Type A1 failures include events where the satellite moves away from its broadcast location due to a commanded maneuver and is known to the GBAS ground facility. The failure class designated as type A2 also includes cases of a satellite maneuver, but without a command being issued by the GPS Operational Control Segment (OCS) and, thus, without an announcement to the GBAS ground facility. Although a possible precedent for this type of event exists in the attitude-control thruster glint firings that have occurred on space vehicles (SVs) 15 and 18 during eclipse seasons and can cause stand-alone user range errors as large as 20 m (Ref. 4), the resulting errors are too small to concern GBAS. To cause errors significant to GBAS, one or more of the more-powerful orbit-maneuvering thrusters would have to fire without being commanded to, and the resulting satellite motion away from its nominal ephemeris would have to go undetected by OCS. Feedback from personnel inside and outside of OCS indicates that the uncommanded firing of one of the larger thrusters is extremely improbable because it cannot be triggered automatically and because multiple failures would have to occur on the satellite.[5]

Type B failures, which are considered to be more credible but still very rare, include all cases where no unscheduled maneuver has occurred, but the ephemeris data broadcast are nevertheless incorrect. This event would most likely be caused either by an error

Received 22 April 2005; accepted for publication 17 October 2005.

*Postdoctoral Researcher, Department of Aeronautics and Astronautics, Durand Building, 496 Lomita Mall.
†Senior Research Engineer, Department of Aeronautics and Astronautics, Durand Building, 496 Lomita Mall.
‡Professor, Department of Aeronautics and Astronautics, Durand Building, 496 Lomita Mall. Member AIAA.
§Assistant Professor, Department of Mechanical, Materials, and Aerospace Engineering, Engineering 1 Building, 10 West 32nd Street. Member AIAA.
¶Research Assistant, Department of Mechanical, Materials and Aerospace Engineering, Engineering 1 Building, 10 West 32nd Street.

in computing the broadcast ephemeris parameters or by corruption of the correct parameters somewhere along the line from OCS creation to OCS satellite uplink to satellite broadcast. Updated GPS navigation data are normally uploaded to each satellite once per day and are composed of 12 frames of data that are cycled through at 2-h intervals, with each ephemeris frame being fit to the satellite orbit over a 2-h interval surrounding its time of ephemeris.[6] Thus, if a type B fault were to occur, it would become evident at the time of switchover from an old (valid) frame to a new (anomalous) one. When this occurs, GBAS ground stations must validate the new data frame and switch from the old to new frame in its computed pseudorange corrections between 2 and 3 min after the new data are received or else exclude the satellite as unhealthy.[7]

GBAS ground systems are required to perform a series of sanity checks on navigation when satellites first rise into view and when data switchovers occur. These monitors are collectively known as data quality monitoring (DQM).[8] These checks confirm that the navigation data themselves do not signal a problem and that the new data are consistent with other data, such as current almanac data or prior ephemeris messages, to within the limits of normal operations. However, for newly rising satellites, the performance of DQM is not sufficient to meet GBAS availability requirements. Moreover, such monitoring is insufficient against type A failures because the preceding data are of no use for the consistency check after a satellite maneuver.

Another key contributor to the sanity checks is the message field range test (MFRT), which simply confirms that the magnitude of the resulting pseudorange corrections is reasonable. Under nominal conditions and with selective availability (SA) off, these corrections (which are basically the difference between measured pseudorange and computed range based on the broadcast ephemeris) should not exceed a magnitude of about 100 m. If they do exceed 100 m, and no other monitor flags have occurred on this satellite, then a large ephemeris error is a strong possibility. This is true for both type A and B failures.[3] However, as already noted, MFRT only observes the component of ephemeris error in the satellite-to-ground-station line of sight; thus, it is not guaranteed to detect all threatening ephemeris errors.

Pervan and Chan proposed a method to detect both type A and B failures based on the use of carrier-phase measurements made by two or more GBAS reference receivers separated by short baselines.[9] An ephemeris anomaly can be directly observed by this spatial separation (a few hundred meters) because the anomaly will cause an effective differential ranging error between receivers that increases in proportion with the baseline length between the receivers. Such a short baseline length, limited by GBAS architectures, causes relative insensitivity to observe orbit errors because an aircraft on final approach will have a displacement from the reference receivers that is generally much larger than the baseline length. Thus, this ephemeris monitor must use measurements with low noise: the GPS carrier phase. The use of carrier-phase measurements requires the successful and timely resolution of carrier-cycle ambiguities for newly rising satellites. This resolution is accomplished by applying a geometry-free widelane approach with a dual-frequency GBAS (still an option for category 3 operations). Therefore, although the proposed monitor provides real-time detection capability for all types of ephemeris errors, it is not applicable to a single-frequency GBAS (the current category 1 operation standard).

This paper has been structured to provide the reader with one coordinated approach to ephemeris monitoring by synthesizing all presently available monitoring schemes. Thus, it includes a brief review of prior methodologies presented in Ref. 10 to monitor GPS satellite ephemeris for the category 1 precision approaches along with a full description of newly proposed methods. This paper is organized as follows. In Sec. II, an overview of the navigation requirements is given. In Sec. III, we develop protection level equations for the ephemeris failure hypothesis that allow GBAS users to compute bounds on possible position errors due to ephemeris failures, provided that the GBAS ground facilities can establish bounds on the magnitude of potentially undetected ephemeris failures. In Sec. IV, a monitor concept to detect type B failures has been developed that is now known as the yesterday-minus-today ephemeris (YE–TE) test. Several variants of this concept are presented in conjunction with experimental results from both nominal and erroneous ephemeris data. In Sec. V, the measurement-based monitor is illustrated, which is designed to detect type A failures and also to confirm that the prior day's ephemeris used in YE–TE is fault free. In Sec. VI, synthesized performance of the YE–TE and measurement-based monitors is discussed. The impact of various ephemeris monitors on system availability is highlighted with the issues of computational cost and architectural design. The paper is summarized in Sec. VII, and some general conclusions are drawn.

II. GBAS Navigation Requirements

As some background on GBAS, we need to introduce the relevant navigation requirements. The four criteria to evaluate the performance of navigation systems are defined as follows:[11,12]

1) The first criterion is accuracy, where a measure of the difference between the estimated position and the true aircraft position under nominal fault-free conditions is made. This is typically a 95% bound on navigation sensor error.

2) The second criterion is integrity, the ability of a navigation system to detect threats and provide warnings to users in a timely fashion.

3) The third criterion is continuity, the ability of the system to support accuracy and integrity requirements throughout a flight operation without interruption.

4) The fourth criterion is availability, the percentage of time for which the system is operational and the accuracy, integrity, and continuity requirements are met.

Integrity fails when a position error exceeds a certain alert limit (AL) and this event is not notified to a pilot within a specified time to alarm. Thus, integrity risk is defined as the probability that no alert is issued while the position error exceeds the AL for a time longer than the time to alarm. In contrast to integrity risk, continuity risk is defined as the probability of the system failing during a specified time interval. Based on the level of these requirements, precision approaches are rated to category 1–3 operations. Categories 2 and 3 involve more stringent requirements, allowing users to operate in lower visibility conditions. In this work, we will focus on the category 1 system. The vertical navigation requirements of this system are summarized in Table 1 (Ref. 13). Because the vertical direction is the most stringent one, and errors in this direction are the worst in general, our focus will be on meeting the vertical requirements.

If hazardously misleading information causes a category 1 user's vertical position error to exceed a 10-m vertical alert limit (VAL), the GBAS ground station must detect the event and alert the user within a 3-s time to alarm. However, the true position and, consequently, the position error, are not quantities that can be known in real time. For that reason protection bounds, defined as protection levels, need to be computed with an acceptable level of integrity risk. The vertical protection levels (VPL) are computed at the aircraft under multiple operational hypotheses, fault-free (VPL_{H0}), single reference-receiver failure (VPL_{H1}), and single satellite ephemeris fault (VPL_e), using the user's satellite geometry information, nominal ranging measurement error models, and range error parameters (derived from integrity monitor performance) broadcast by the ground station. If VPL exceeds the VAL, the system is no longer available. Because this paper concentrates on monitoring satellite orbit errors, more details on VPL_e will be given in the next section.

Table 1 Requirements for category 1 precision approach

Requirement	Value
Vertical accuracy, 95% error	4–7.6 m
Integrity risk	
Pr(HMI)	2×10^{-7}/approach
Time to alert	3 s
Continuity risk	5.5×10^{-5}/approach
Availability	0.99–0.99999
Vertical alert limit	10–12 m

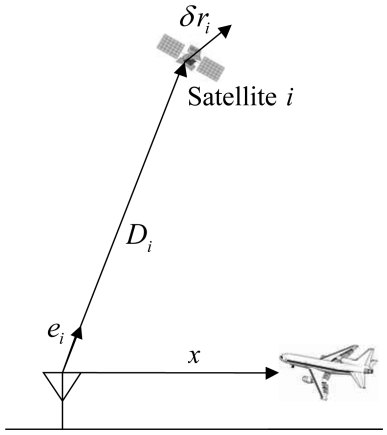

Fig. 1 Satellite, reference station, and user relative geometry.

III. Ephemeris Protection Levels and Availability Impact

To quantify the potential impact of undetected ephemeris failures on user position errors for both precision approach and terminal area applications, new protection levels must be adopted. These equations define position error bounds as functions of the approximate aircraft location with respect to each satellite and the GBAS ground station as well as the magnitude of the satellite orbit error detectable by the ground station. This minimum detectable error (MDE) determines the P-value (definition to be given shortly), which is broadcast by the GBAS ground station for each satellite it has approved for use. In this section, we derive the ephemeris protection level (VPL_e) and discuss its impact on GBAS availability.

The effective differential ranging error $\delta\rho$ due to an error δe in knowledge of the line-of-sight unit vector $\boldsymbol{e}$ for some satellite i is

$$\delta\rho_i = \delta\boldsymbol{e}_i^T\boldsymbol{x} \tag{1}$$

where $\boldsymbol{x}$ is the displacement vector between the reference station and user (aircraft) antennas. In turn, the line-of-sight vector error can be expressed directly in terms of the satellite position error vector δr_i as

$$\delta\boldsymbol{e}_i = \left(\boldsymbol{I} - \boldsymbol{e}_i\,\boldsymbol{e}_i^T\right)\delta\boldsymbol{r}_i \Big/ D_i \tag{2}$$

where D_i is the distance (scalar) to satellite i as shown in Fig. 1. Substituting Eq. (2) into Eq. (1), we have

$$\delta\rho_i = \delta\boldsymbol{r}_i^T\left(\boldsymbol{I} - \boldsymbol{e}_i\,\boldsymbol{e}_i^T\right)\boldsymbol{x}\Big/ D_i \tag{3}$$

When this error and the other remaining (nominal) error sources (vector $\boldsymbol{\nu}_p$ given hereafter containing ground, air, ionospheric, and tropospheric errors) are projected into the user position domain, the resulting position estimate error for the vertical direction will be

$$\delta\chi_{\mathrm{vert},i} = S_{\mathrm{vert},i}\left[\delta\boldsymbol{r}_i^T\left(\boldsymbol{I} - \boldsymbol{e}_i\boldsymbol{e}_i^T\right)\boldsymbol{x}\Big/ D_i\right] + S_{\mathrm{vert},:}\boldsymbol{\nu}_p \tag{4}$$

where $S_{\mathrm{vert},:}$ is the row of the weighted-least-squares projection matrix corresponding to the vertical position state.[7] We consider the vertical case only in this development; the development for the horizontal case is essentially identical.

When the first term in Eq. (4) is written, it is assumed that ephemeris failures occur on only satellite i. (We assume that the probability of simultaneous ephemeris failures on more than one satellite is negligibly small.) For brevity in notation, we define the 3×3 matrix $E_i \equiv I - e_i e_i^T$. It is also noted that $\delta r_i^T E_i x$ is a scalar and that

$$\delta\boldsymbol{r}_i^T E_i\boldsymbol{x} \le \|E_i\boldsymbol{x}\|\|\delta\boldsymbol{r}_i\| \tag{5}$$

We assume now that we have a test statistic t_e available at the reference station, that is, almanac-minus-ephemeris position difference, that we may use to infer orbit error magnitude. In this case, a threshold T_e on the test statistic may be defined to detect and exclude (at the reference station) a satellite with a large orbit error

$$T_e = k_{\mathrm{FFA}}\sigma_{t_e} \tag{6}$$

Here, σ_{t_e} is the standard deviation of the nominal test statistic, and k_{FFA} is a multiplier defined to ensure a specified probability of fault-free alarm (FFA). If we define ν_{t_e} to be a zero-mean, normally distributed random variable with σ_{t_e}, it is always true that

$$\|\delta\boldsymbol{r}_i\| < T_e + \nu_{t_e} \tag{7}$$

Substituting Eqs. (5), (6), and (7) into Eq. (4), we obtain the following bound on vertical position error:

$$|\delta\chi_{\mathrm{vert},i}| \le |S_{\mathrm{vert},i}|(\|E_i\boldsymbol{x}\|/D_i)k_{\mathrm{FFA}}\sigma_{t_e} + |S_{\mathrm{vert},i}|(\|E_i\boldsymbol{x}\|/D_i)\nu_{t_e} + |S_{\mathrm{vert},:}\boldsymbol{\nu}_p| \tag{8}$$

Note that ν_{t_e} is a scalar whereas $\boldsymbol{\nu}_p$ is a vector. The standard deviation of the random part of $\delta\chi_{\mathrm{vert},i}$, that is, the second and third terms in Eq. (8), is the left-hand side of Eq. (9), and the following inequality is obtained:

$$\sqrt{S_{\mathrm{vert},i}^2\frac{\|E_i\boldsymbol{x}\|^2}{D_i^2}\sigma_{t_e}^2 + \sum_{j=1}^{n}S_{\mathrm{vert},j}^2\sigma_j^2} \le |S_{\mathrm{vert},i}|\frac{\|E_i\boldsymbol{x}\|}{D_i}\sigma_{t_e} + \sqrt{\sum_{j=1}^{n}S_{\mathrm{vert},j}^2\sigma_j^2} \tag{9}$$

where σ_j is the standard deviation of the jth element of $\boldsymbol{\nu}_p$, and n is the number of satellites used in the position fix. Furthermore, it is also true that

$$\|E_i\boldsymbol{x}\| \le \|\boldsymbol{x}\| \tag{10}$$

We next define a missed detection (MD) multiplier k_{MD} based on the assumed prior probability of ephemeris error and the tolerable total level of integrity risk. Together with Eqs. (8–10), where we add the first term in Eq. (8) and the right-hand side of Eq. (9) multiplied by k_{MD}, we can now write an upper bound on vertical position error, which we call $\mathrm{VPL}_e(i)$, or the VPL under the ephemeris failure hypothesis for satellite i

$$\mathrm{VPL}_e(i) = |S_{\mathrm{vert},i}|\frac{(k_{\mathrm{FFA}}+k_{\mathrm{MD}})\sigma_{t_e}}{D_i}\|\boldsymbol{x}\| + k_{\mathrm{MD}}\sqrt{\sum_{j=1}^{n}S_{\mathrm{vert},j}^2\sigma_j^2} \tag{11}$$

Within this expression, we have the MDE in satellite position,

$$\mathrm{MDE} = (k_{\mathrm{FFA}}+k_{\mathrm{MD}})\sigma_{t_e} \tag{12}$$

The reference station will broadcast (for each satellite) an ephemeris error decorrelation parameter P_i (Refs. 7 and 14),

$$P_i = \mathrm{MDE}/D_i \tag{13}$$

so that

$$\mathrm{VPL}_e(i) = P_i|S_{\mathrm{vert},i}|\|\boldsymbol{x}\| + k_{\mathrm{MD}}\sqrt{\sum_{j=1}^{n}S_{\mathrm{vert},j}^2\sigma_j^2} \tag{14}$$

At the aircraft, VPL_e is computed as

$$\mathrm{VPL}_e = \max_i \mathrm{VPL}_e(i) \tag{15}$$

In addition to VPL_e, GBAS users also compute vertical protection levels under the fault-free ($H0$) hypothesis.[7] If ephemeris protection levels are large enough to exceed these nominal-case protection levels (VPL_{H0}), they will reduce user availability. The degree to which

this occurs is a function of the P value derived from the MDE of the ground monitors and the location of users relative to the ground station. The most critical user location is when the aircraft reaches the end of its approach (the approach threshold), where the tightest VAL (10 m for category 1) applies.[15] Note that the displacement $x_{\mathrm{RR-GPIP}}$ between the centroid of the reference receivers (RR) and the glide path intercept point (GPIP) is needed to define x in Eq. (14). Given the condition that $x_{\mathrm{RR-GPIP}}$ is fixed, the key factor to keep VPL_e small is to ensure that the ephemeris monitor MDE is small.

A study of the impact of VPL_e on GBAS category 1 availability was reported.[16] For $x_{\mathrm{RR-GPIP}} = 3$ n mile (about 5.5 km), which should suffice for most airports, there is no availability impact, that is, VPL_e is smaller than VPL_{H0} for MDE ≤ 1900 m. Above this value, a slight loss of availability appears but does not become significant until the MDE reaches 4000 m or so. This conclusion was based on $k_{\mathrm{MD}} = 3.7$. Further analysis by Shively has shown that $k_{\mathrm{MD}} = 3.1$, providing a missed-detection probability of 0.001, is acceptable for the ephemeris integrity monitor[17]; thus, the actual MDE that will cause availability loss is somewhat higher. These results provide guidance regarding the ephemeris MDE that will be acceptable in operation. The monitoring methods developed in the following sections are intended to reduce the ephemeris MDE such that little if any GBAS availability is lost.

IV. YE–TE Monitor for Type B Anomalies

The concept of the YE–TE test is simply to confirm that today's broadcast ephemeris data for each GPS satellite are correct by comparison with the most recent ephemeris data that have already been validated. For a satellite that is already in view and has an ephemeris frame change, the comparison is between the new and immediately preceding sets of data. Under nominal conditions, these agree to within several meters during the 2-h period within the fit intervals of both sets of data.[3] However, when a satellite first rises in view of the GBAS ground station, the most recent validated data are from the preceding pass of that satellite and may be as much as 24 h old. Thus, it is long past its fit interval and no longer precisely indicates the satellite location. Nevertheless, it is a valid basis for comparison within the limits of its accuracy. If the new ephemeris is dramatically in error, as in the type B failure defined in Sec. I, this comparison will detect the failure. This nonfit YE–TE method is detailed in Sec. IV.A. By applying an orbit determination method, we can improve the accuracy of satellite position estimates and consequently reduce the MDE. This orbit-fitting YE–TE method is explained in Sec. IV.B. YE–TE comparisons can be based on not only satellite positions computed from the old and new ephemerides but also the individual orbit parameters of the old and new messages. The latter approach, parameter-based YE–TE, is explained in Sec. IV.C. Note that the focus of all three methods is on detecting type B anomalies for newly risen satellites assuming the yesterday's ephemeris data are valid.

The impact of incorrectly rejecting a satellite with a healthy ephemeris is that the use of a healthy satellite is lost, but continuity is not affected because rejection would occur before the satellite is approved for use that day. Therefore, the YE–TE FFA probability need not be low enough to fit within the continuity allocation. (See Sec. II.) Instead, it should be small compared to the probability that a given satellite will be flagged unhealthy (and, thus, unusable) when it rises into view. Based on prior analyses by Pullen,[18] probability FFA [Pr(FFA)] can be set to 1.9×10^{-4} per newly risen satellite, which gives $k_{\mathrm{FFA}} = 3.73$, provided that a Gaussian extrapolation can be used. During ephemeris changeovers for already-approved satellites, continuity is at risk if the satellite is rejected; thus Pr(FFA) must fit within the overall continuity requirement of 8×10^{-6} per 15 s (Ref. 14). The nominal ephemeris differences are much lower in this case; thus, this lower Pr(FFA) does not require an increase in MDE.

A. Nonfit YE–TE Monitor

The algorithm is as follows. First, compute satellite positions using the standard algorithm defined in Sec. 20.3.3.4.3 of GPS ICD-200D (Ref. 19) and GPS ephemeris parameters. These satellite positions computed in the Earth-centered Earth-fixed reference frame are then rotated into the in-track–cross-track–radial or local level orbit-referenced frame. Two satellite position vectors are calculated using the current and previously validated ephemeris parameters. We define $\boldsymbol{r}_{\mathrm{TE}}(k)$ as a vector containing the three components of the position of a given satellite at epoch k, based on the latest (to-be-validated) ephemeris, and define $\boldsymbol{r}_{\mathrm{YE}}(k)$ similarly but based on the preceding already-validated ephemeris. A YE–TE position-difference vector in each axis can be created for a vector of epochs that covers the visibility period of interest,

$$\delta\hat{\boldsymbol{r}}(k) = \boldsymbol{r}_{\mathrm{TE}}(k) - \boldsymbol{r}_{\mathrm{YE}}(k), \qquad k = 0, 1, \ldots, n \tag{16}$$

Second, the maximum of $\delta\hat{r}$ in each axis over the time period covered by k is the test statistic for that axis. Thresholds can be set individually for each axis from each test statistic ($t_{e\_\mathrm{in-track}}$, $t_{e\_\mathrm{cross-track}}$, and t_{e_radial}), or the three-dimentional test statistic t_e, the rss of maximum position differences for each axis, can be used to derive a single threshold. [See Eq. (6).] The latter is more convenient because it directly translates into the scalar MDE value used to compute VPL_e [see Eq. (12).] Last, the test statistic t_e will be compared to the threshold T_e to detect an anomalous ephemeris.

The algorith results are as follows. Figures 2–4 show plots of the in-track, cross-track, and radial components of orbit differences, respectively. The satellite positions computed from ephemerides received at the Colorado Springs international GNSS service (IGS) site amc2 on 10 January 2001 are compared to those computed from ephemerides with a time of ephemeris t_{OE} 24 h earlier. In each case, the epoch k runs from the t_{OE} of the new ephemeris, $k = 0$ at t_{OE} of TE, to a time 8 h later (long enough to cover any satellite pass) at 5-min intervals. Under nominal conditions, the position differences shown in Figs. 2–4 are due to orbit perturbations that take place during the period from t_{OE} of YE to t_{OE} of TE. Note that

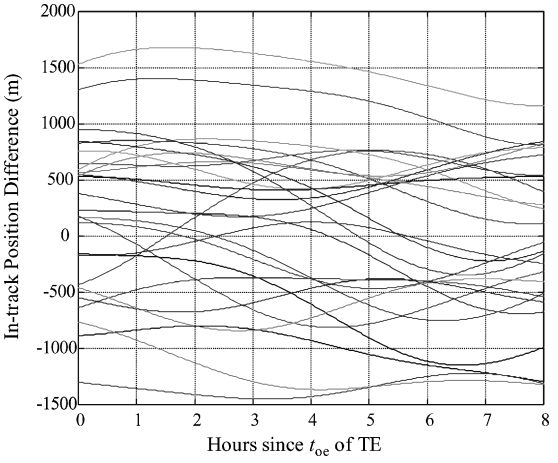

Fig. 2 Example YE–TE results for in-track axis.

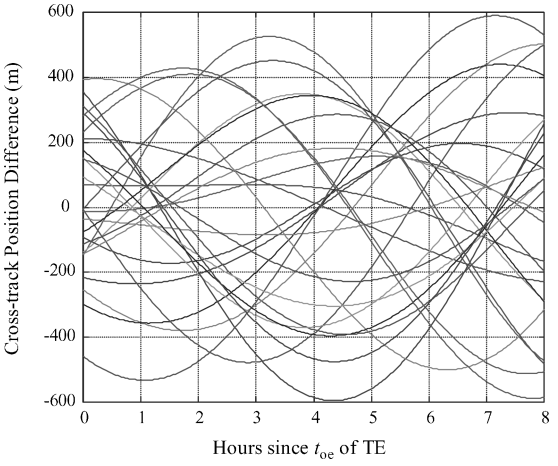

Fig. 3 Example YE–TE results for cross-track axis.

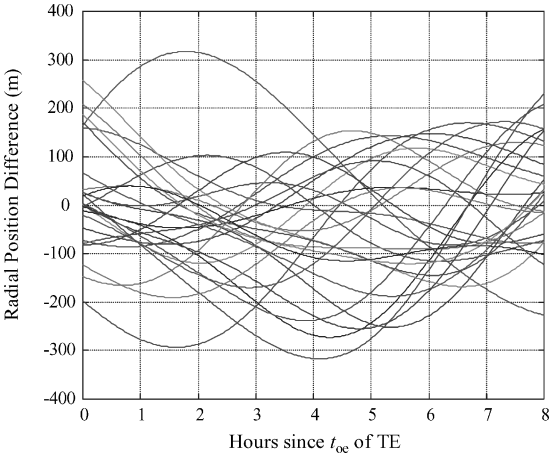

Fig. 4 Example YE–TE results for radial axis.

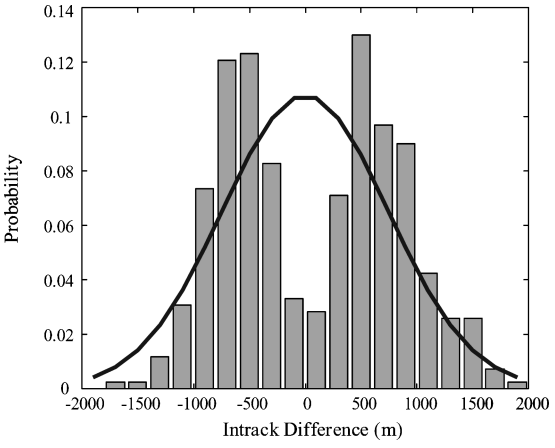

Fig. 5 YE–TE histogram for in-track axis.

nominal ephemeris messages are very accurate only within their fit intervals (±2 h from t_{OE}, Ref. 2). The in-track differences are the largest and, therefore, dominate the combined test statistic t_e. (Note that the in-track differences vary within about ±1500 m in Fig. 2, whereas the differences in cross-track and radial directions oscillate within approximately ±600 and ±300, respectively, in Figs. 3 and 4.) Whereas the cross-track and radial differences are dominated by short-period oscillations with periods of less than a day, the in-track differences show both short and long-period oscillations. (The long-period oscillations dictate the nonzero mean of the in-track differences.)

Figure 5 shows a histogram of orbit differences in the in-track axis for all valid satellite ephemerides received at Colorado Springs from 7 January through 17 February 2001, a total of 423 separate YE–TE test results. Satellites undergoing maintenance (and possible orbit changes) were excluded from these results based on information issued by OCS. Note that the test statistic distributions are bimodal; typical values are on either side of zero rather than centering about zero. However, the Gaussian distribution with zero mean and the sample standard deviation (746.2 m in Fig. 5 where the cross-track and radial values are 398.9 and 165.6 m, respectively) shown as a solid line appears to overbound the observed bimodal distributions in the tails. Thus, a threshold and MDE derived from the Gaussian extrapolations in Eqs. (6) and (12), respectively, should be applicable. The resulting threshold is 3216 m, and the MDE is 5889 m for this test. This demonstrates that the nonfit monitor produces some availability loss, MDE > 4000 m. Further discussion on availability impact will be given in Sec. VI.

B. Orbit-Fitting YE–TE Monitor

The algorithm is as follows. The YE–TE method defined in Sec. IV.A is based on the direct comparison of satellite positions computed from the old and new ephemerides without any attempt to predict satellite orbit changes from yesterday to today. In theory, a more accurate method is to model directly the expected perturbations using orbit theory. Estimating the position and velocity of a dynamic trajectory from a set of tracking observations is called orbit determination. When tracking observations are not available, dynamic models, the mathematical models that describe the satellite force environment, are used to predict the motion of a spacecraft. In this work, we use the satellite locations computed from the YE during its 4-h fit interval as measurements for the orbit determination. This orbit fitting is highly accurate because the input observations were accurate to within a few meters in three dimensions, based on nominal GPS ephemeris accuracy, if YE was valid the preceding day. Dynamic orbit-perturbation models are then used to fill in the gap between the time of applicability of YE and today's t_{OE} so that a projected satellite position estimate $\hat{r}_{YE}$ is available to compare to the satellite position r_{YE} computed from the TE. As with the nonfit YE–TE monitor, a YE–TE position-difference vector is generated for a vector of epoch k:

$$\delta\hat{\boldsymbol{r}}(k) = \boldsymbol{r}_{TE}(k) - \hat{\boldsymbol{r}}_{YE}(k), \qquad k = 0, 1, \ldots, n \tag{17}$$

Again, the maximum of $\delta\hat{r}$ in each axis over the time period covered by k is the test statistic t_e for that axis. This test statistic is then compared to the detection threshold T_e. The dynamic models are usually associated with inaccuracies, and the residual pattern will show some mean biases. Thus, we have

$$T_e = \left|\mu_{t_e}\right| + k_{FFA}\sigma_{t_e} \tag{18}$$

where μ_{t_e} and σ_{t_e} are the mean and standard deviation of the nominal test statistic, respectively, and k_{FFA} is a multiplier defined to provide a specified probability of FFA. If, in fact, the dynamic models are quite accurate, the orbit difference will simply exhibit the random component in the measurement. [In such cases, a distribution with zero-mean can be assumed, and Eq. (6) is used to derive the threshold.] Based on a required probability Pr(MD), the MDE is

$$\text{MDE} = \left|\mu_{t_e}\right| + (k_{FFA} + k_{MD})\sigma_{t_e} \tag{19}$$

where k_{MD} is the probability multiplier associated with Pr(MD).

The sensitivity analysis is carried out as follows. The orbit-fitting method considerably improves the accuracy of satellite position estimates compared to the nonfit or parameter-based methods, which will be shown shortly. However, it would be complex and expensive to implement in a real-time GBAS ground station. To minimize computational burden, it is important to investigate the sensitivity of satellite position errors to complexities of dynamic models. The dynamic models, used to propagate the satellite position and velocity between measurement epochs, are always approximations of the actual forces acting on the satellite. If the dynamic model is not accurate enough to predict the satellite motion, the filter in an orbit determination method may diverge. On the other hand, the complex dynamic model can worsen the speed of integrating the satellite equations of motion numerically, while improving the orbit accuracy. Thus, balancing the accuracy requirements and the computational cost of the propagator is required.

To implement several orbit-fitting variations, we utilized Microcosm®, which is the precision orbit and geodetic parameter estimation software system.[20] Microcosm applies Cowell's method, the direct numerical integration of the satellite equation of motion in rectangular coordinates, to predict the orbit and Bayesian least-squares estimation for parameter determination. The batch mode of estimation is used in Microcosm, and iteration is performed both to facilitate automatic data editing and because of the nonlinearity of the orbit determination problem. The acceleration producing forces that are currently modeled in Microcosm are the effects of the geopotential, the lunar–solar potential, planetary potentials, radiation pressure, Earth tide potential, atmospheric drag, and general relativistic perturbation. The solar radiation pressure model employed here is an empirical model based on experimental measurements and

Table 2 Case study of different dynamic models

Case	Geo-potential	Lunar–solar potential	Planetary potentials	Direct solar radiation pressure	Solid Earth and ocean tide	Atmospheric drag	General relativistic effect
1	12×12	On	Off	On	On	On	Off
2	6×6	On	Off	Off	Off	On	Off
3	12×12	On	Off	Off	On	On	Off
4	12×12	On	Off	On	Off	On	Off
5	6×6	On	Off	On	Off	On	Off
6	4×4	On	Off	On	Off	On	Off
7	3×3	On	Off	On	Off	On	Off
8	3×2	Off	Off	On	Off	On	Off

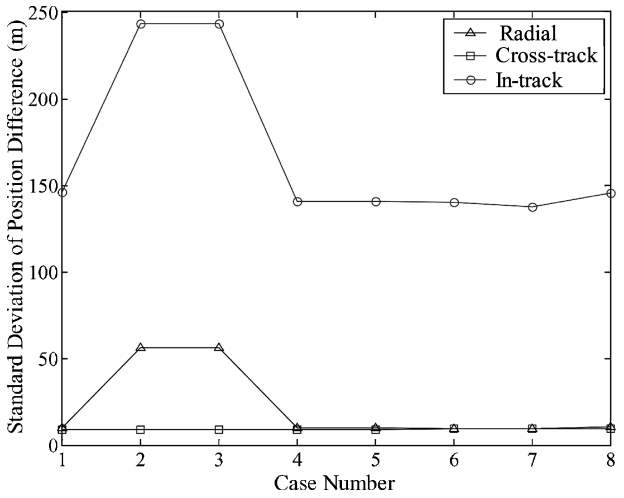

Fig. 6 Standard deviation of position difference for different dynamic models.

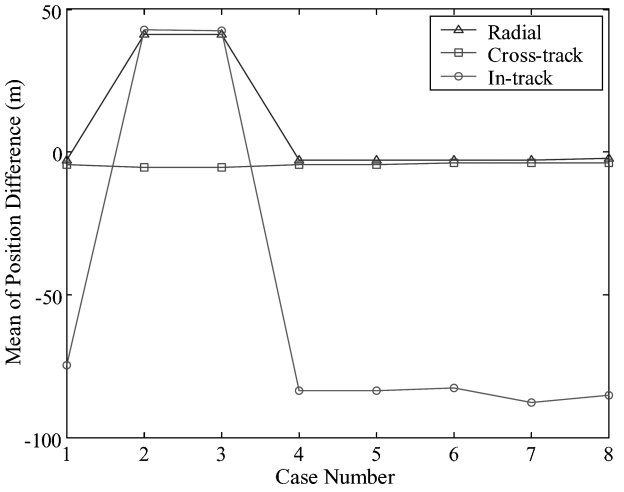

Fig. 7 Mean of position difference for different dynamic models.

numerical simulations of the reflective surfaces of the NAVSTAR Global Positioning System Block C.

When various accelerations are modeled or unmodeled, eight different case studies (as shown in Table 2) have been performed to find the least-complex orbit model that provides the needed performance. First, the satellite positions computed from TE are compared to those computed by propagating ephemeredes with a t_{OE} 24 h earlier (YE) to the t_{OE} of TE. The YE–TE position-difference vector $\delta\hat{r}(k)$ runs from the t_{OE} of TE, $k = 0$, to a time 8 h later at 1-min intervals. As explained earlier, we then take the maximum of $\delta\hat{r}$ over this time period, which is the test statistic for each axis. Last, we compute standard deviation, mean, and rms values for this test statistic. This process is repeated for each case, which represents the different propagator used in orbit determination as specified in Table 2.

Figures 6 and 7, respectively, show the standard deviation and mean of orbit differences in the in-track, cross-track, and radial axes for each case. The results for each case are generated from 30 YE–TE pairs between 9 January and 12 January 2001. For case 8, applying the orbit-fitting technique to create $\hat{r}_{YE}$ reduces the cross-track and radial YE–TE values to about 10 m (1σ) and makes them negligible compared to the in-track YE–TE value, which has an rms value of 166.3 m. (This technique also removes most of the long-period oscillation.) A mean offset of about -85 m in the in-track axis is visible in Fig. 7 and consistently appears in data from other days in January. Subtracting this offset from the test statistic leaves a standard deviation of 145.3 m. Because the results are no longer strongly bimodal, a Gaussian extrapolation with $k_{FFA} = 3.73$ and $k_{MD} = 3.1$ can be used with Eq. (19) to derive an MDE of about $1000 \sim 1100$ m for this test. Validation with more data will be shown shortly.

Based on the preceding result, a 3×2 expansion of the standard joint gravity model version 3 (JGM-3) Earth gravity model combined with the Microcosm solar radiation pressure and atmospheric drag models (case 8) is sufficient to achieve the needed orbit-determination accuracy. Cases 2 and 3 show that modeling of the solar radiation pressure is the most critical for this experiment. The results from the rest of the cases demonstrate that including planetary potentials, Earth and ocean tide potentials, sun and moon gravity perturbations, and general relativistic perturbation does not significantly improve the resulting YE–TE values.

The results are as follows. This method has been evaluated using the NASA Goddard Space Flight Center GPS Enhanced Orbit Determination (GEODE) software[21] and was implemented in the Stanford Integrity Monitor Test-Bed (IMT),[8] which is used to insure that the GBAS ground facility meets its requirements for navigation integrity. GEODE is highly modular due to its object-based architecture with encapsulated interfaces and is portable because it is programmed in ANSI Standard C. Thus, this software is most suitable to be hosted in the IMT. GEODE employs an extended Kalman filter, which incorporates accurate dynamic models, to estimate orbit state vectors.[22] To reduce computational cost by adding the orbit-fitting YE–TE monitor to the IMT, modifications are made to GEODE to utilize the least-complex dynamic model based on the results of the sensitivity analysis discussed earlier.

Figure 8 shows the MDE as a function of time intervals between t_{OE} of YE and t_{OE} of TE, that is, durations of orbit propagation to generate $\hat{r}_{YE}$. The results are generated from a data set collected from 6 May through 9 May 2002. Each bin consists of about 30 YE–TE pairs (total of 149 YE–TE pairs). As expected, the standard deviation of orbit differences increases as the satellite's ephemeris is propagated longer. This is because errors in the mathematical model accumulate during the period from t_{OE} of YE to t_{OE} of TE. When the time length of propagation is about 25 h, the resulting standard deviations of YE–TE are 151.3, 20.7, and 46.2 m, and the means of YE–TE are -53.0, 4.1, and -16.7 m in the in-track, cross-track, and radial axes, respectively. When Eqs. (18) and (19) are used, a threshold of 651 m and an MDE of 1145 m are derived for this test. Thus, this monitor significantly reduces the MDE compared to other YE–TE variants explained earlier and causes no availability loss (MDE $<$ 1900 m).

To validate the analytically derived MDE, controlled errors are injected into nominal ephemeris parameters. As shown in Eq. (20),

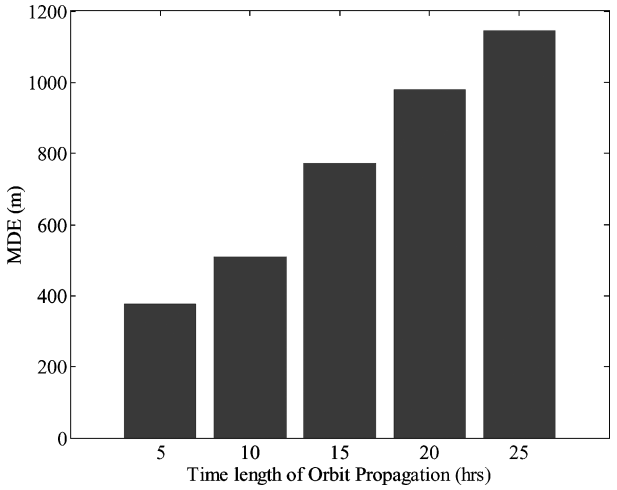

Fig. 8 Minimum detectable errors of orbit-fitting YE–TE monitor.

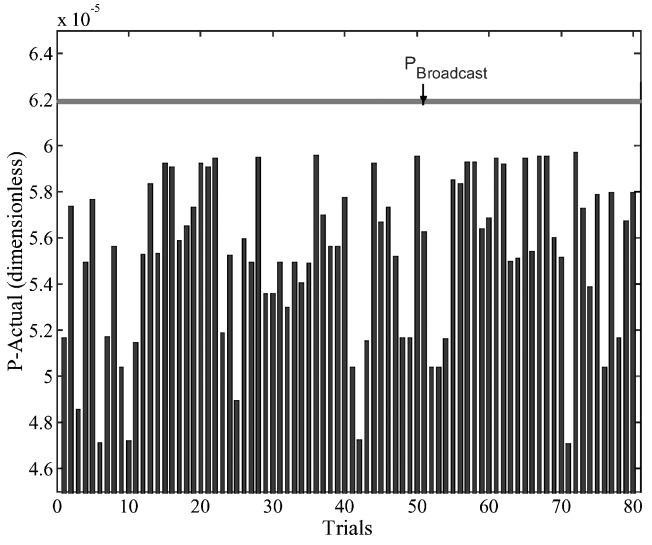

Fig. 9 P_{actual} results from failure test with an error of 0.0375 injected on $\sqrt{a}$.

the true position error δr can be computed by generating position solutions first with the fault-free parameters g and then with erroneous parameters caused by an introduced error δg,

$$\delta \boldsymbol{r} = \boldsymbol{r} - \boldsymbol{r}_{\text{faulty}} = \boldsymbol{r}(g) - \boldsymbol{r}(g + \delta g) \tag{20}$$

When these true position errors are used, the actual P values P_{actual} can be computed as [which is the same as Eq. (2)]

$$P_{\text{actual}} = \left(\boldsymbol{I} - \boldsymbol{e}_i \boldsymbol{e}_i^T\right) \delta \boldsymbol{r}_i \Big/ D_i \tag{21}$$

where e_i is the line-of-sight unit vector for satellite i and D_i is the distance from a reference station to satellite i. Recall that the parameter P, depending on the ground ephemeris monitor implementation, will be broadcast to the aircraft for computing their VPL_e. When the shortest possible range from the Earth's space to a satellite (approximately 20,184 km) and the MDE of 1250 m are conservatively taken, the broadcast P value is

$$P_{\text{broadcast}} = \frac{\text{MDE}}{r_{\min}} = \frac{1250}{20{,}184{,}000} = 6.193 \times 10^{-5} \tag{22}$$

To ensure navigation integrity, it is desired that $P_{\text{actual}} < P_{\text{broadcast}}$; otherwise, the aircraft may not be protected with their VPL_e in the event of ephemeris failure.

Figure 9 shows the result of an empirical analysis under failure conditions. An error of 0.00375 square-root meters was added on the square root of the semimajor axis $\sqrt{a}$. This parameter fault is deliberately introduced to cause errors in the satellite position of a magnitude similar to the MDE of 1250 m. The bars show the actual P values P_{actual} computed from 80 erroneous orbits, and the straight line shows the broadcast P value $P_{\text{broadcast}}$ of this orbit-fitting YE–TE monitor. The P_{actual} is always overbounded by the $P_{\text{broadcast}}$ in this test, which verifies that the derived $P_{\text{broadcast}}$ and MDE values are conservative enough to meet integrity requirements. In failure tests where faults were injected on various ephemeris parameters (one parameter at a time), very similar results were obtained, and P_{actual} never exceeded $P_{\text{broadcast}}$.

C. Parameter-Based YE–TE Monitor

The YE–TE implementations considered thus far have involved tests in the satellite position domain. An alternative YE–TE approach is based on the direct comparison of current broadcast ephemeris parameters with those broadcast and validated earlier. The advantage of a parameter-based approach is that it is easier to observe and quantify variations in orbit parameters than satellite position because the latter changes continuously in time for a fixed parameter set. The parameter-based approach provides improved performance over the nonfit YE–TE algorithm (Sec. IV.A), while offering a lower level of complexity than the orbit-fitting YE–TE approach (Sec. IV.B). Furthermore, the performance of this test can also be easily expressed in position domain, which is needed to define the MDE and P value. In this section, the algorithms and test results, which have been fully described in prior work,[10] are summarized. The end result and performance of the parameter-based YE–TE method will be compared with those of position-based YE–TE monitors in Sec. VI.

The algorithm is as follows. This method attempts to predict satellite orbit changes by estimating the variations in the broadcast ephemeris parameters from the last available validated ephemeris. We first generate the satellite position vector r_{TE} for different epochs k corresponding to the broadcast period, using the current ephemeris that we are trying to validate. Second, the satellite position estimate $\hat{r}_{\text{YE}}$ is computed using the best estimate available based on earlier validated ephemerides. The position error estimate $\delta\hat{r}$ is then

$$\delta\hat{\boldsymbol{r}}(k) = \boldsymbol{r}_{\text{TE}}(k) - \hat{\boldsymbol{r}}_{\text{YE}}(k) \tag{23}$$

Because the daily variations of each broadcast parameter follow a recognizable pattern (usually with a sinusoidal shape), it is advantageous to consider estimators based on prior days of data. Thus, the parameter-based YE–TE method is implemented via two parameter-projection algorithms: the zero-order hold (ZOH) and first-order hold (FOH) estimators. The FOH applies a linear projection on parameter estimation based on two prior days of data and, thus, partially captures the nature of the day-by-day variations in the parameters that are unaccounted for in the ZOH.

A normalized test statistic,

$$s = \delta\hat{r}^T \Sigma_{\delta\hat{r}}^{-1} \delta\hat{r}$$

where $\Sigma_{\delta\hat{r}}$ is the covariance matrix, is computed and is compared to a threshold T_e that ensures the required probability of FFA. The MDE is defined as

$$\text{MDE} = \sqrt{\lambda q} \tag{24}$$

where λ is the minimum noncentrality parameter that satisfies the required probability of missed detection and q is the maximum eigenvalue of $\Sigma_{\delta\hat{r}}$ (See Ref. 10 for details.) The values in the covariance matrix of the FOH estimator are significantly smaller than those for the ZOH, showing a higher accuracy in satellite position estimation $\hat{r}_{\text{YE}}$. This allows smaller MDE values, avoiding a significant loss in availability.

The results are as follows. Figure 10 shows the fault-free distributions of satellite position errors $|\delta\hat{r}(0)| = |r_{\text{TE}}(0) - \hat{r}_{\text{YE}}(0)|$ achieved by applying the two different parameter projection methods for a 1-year span of ephemeris data. The FOH estimator yields a much tighter distribution of fault-free errors than the ZOH estimator. Based on these distributions of test statistics, the MDEs for the

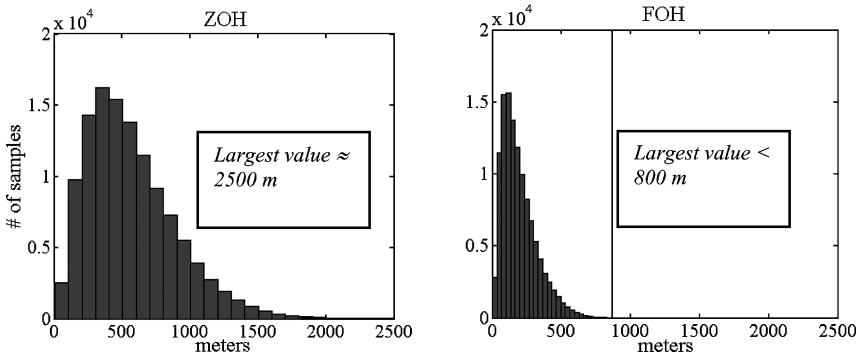

Fig. 10 ZOH and FOH position error, $|\delta\hat{r}|$, distributions.[10]

ZOH and FOH monitors were computed. The results show that $\mathrm{MDE_{ZOH}} = 4984$ m and $\mathrm{MDE_{FOH}} = 1744$ m.

Despite the better performance of the FOH, the principle drawback is that it requires two prior days of ephemerides, whereas the ZOH needs only one. Consequently, a procedure to support that the prior day's ephemeris is fault free should be executed twice for the FOH. The downside effect toward a total MDE will be discussed in Sec. VI.

To verify fault detection ability of the monitor, failure tests were performed by deliberately injecting anomalous parameters in otherwise nominal ephemeris broadcasts. The sizes of anomalies were chosen to cause satellite position errors of magnitudes similar to the derived MDE values. For both the ZOH and FOH estimators, the percentage of missed detections was significantly lower than a required value of 10^{-3}.

V. Measurement-Based Monitor for Type A Anomalies

The implicit assumption in any YE–TE implementation is that prior ephemeris data is fault free. Thus, to utilize YE–TE monitors, a method to support the fault-free assumption on a daily basis is necessary. Regardless of the particular YE–TE implementation used, after a scheduled station-keeping maneuver (type A1 failures), no valid prior ephemeris will be available to test current broadcast ephemeris. In this case, a new method to validate the postmaneuver ephemeris message, that is, the broadcast ephemeris on the day immediately following a satellite maneuver, is needed. (Type A2 failures are considered to be sufficiently improbable that no targeted monitor for these is required to meet the integrity requirements of category 1 precision approach.[15]) For theses cases, a measurement-based monitor can fulfill the objective by directly using GBAS code and carrier measurements. Here we provide a brief description of the monitoring algorithm and results of achievable MDEs that will provide a total MDE when combined with those of YE–TE monitors. More detail on this monitor is shown in Ref. 10.

The basic idea of the measurement-based monitor is to relate the magnitude of the stand-alone pseudorange and the differential carrier-phase residuals to the magnitude of satellite orbit errors. The stand-alone pseudorange residual, that is, the broadcast pseudorange correction that measures the orbit error (at epoch k) projected into the satellite's line-of-sight direction e, can be written

$$z^{\rho}(k) = \boldsymbol{e}^{T}(k)\delta\boldsymbol{r}(k) + \upsilon^{\rho}(k) \tag{25}$$

where the measurement error is distributed as $\upsilon^{\rho}(k) \sim N(0, \sigma_{\rho}^{2})$. The differential carrier residual (across GBAS reference receiver baselines) that measures orbit errors orthogonal to the line of sight and projected into a known baseline direction can be expressed as

$$z^{\phi}(k) = \ell[\boldsymbol{d}^{T}E(k)/D(k)]\delta\boldsymbol{r}(k) + \Delta\tau(k) + N\lambda + \upsilon^{\phi}(k) \tag{26}$$

where ℓ is the baseline length, $\boldsymbol{d}$ is the baseline direction unit vector, $E \equiv I - ee^{T}$, I is the 3×3 identity matrix, $\Delta\tau$ is the clock offset between receivers, N is the carrier integer cycle ambiguity, λ is the L1 carrier wavelength (19.04 cm), and υ^{ϕ} is the measurement error due to receiver thermal noise and multipath. The receiver clock offset is easily removed by differencing against a nominal satellite that has not been maneuvered and has passed all recent monitor tests. Thus, this term will not be considered further in the analysis. The cycle ambiguities can be rounded to the nearest integer because the standard deviation of the error in the cycle ambiguity estimates is significantly lower than 10^{-2} carrier wavelengths. (This is based on covariance analysis results with measurements collected for a whole satellite pass.) Therefore, the cycle ambiguities are assumed to be resolved and removed from the differential carrier phase measurement, making $N = 0$ in Eq. (26).

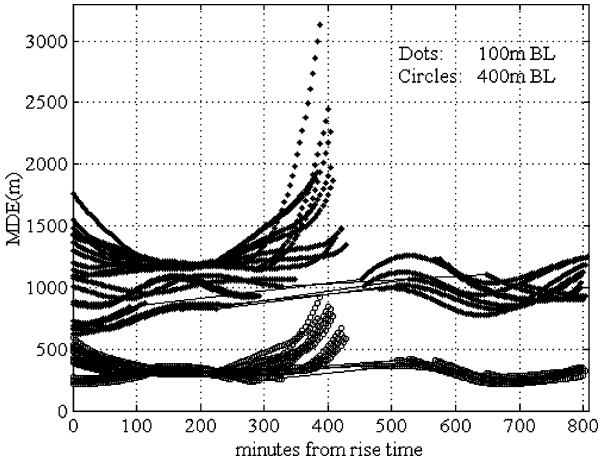

Fig. 11 MDE vs time for all satellites.[10]

To determine the satellite position error δr we first stack the available measurements corrected over a day for the two baselines. (We assume that one day is available to verify the current ephemeris.)

$$z = H\delta\boldsymbol{r} + \upsilon \tag{27}$$

where H is a mapping matrix and the measurement error is distributed as

$$\upsilon \sim N(0, V), \qquad V = \left[\begin{array}{c|c} V^{\rho} & 0 \\ \hline 0 & I\sigma_{\phi}^{2} \end{array}\right] \tag{28}$$

where σ_{ϕ} is the standard deviation of the differential carrier phase measurement error and the submatrix V^{ρ} accounts for the time correlation of pseudorange measurements. (See Ref. 10 for details.) The value of differential carrier error standard deviation is chosen to be consistent with GBAS integrated multipath limiting antenna performance[23]: $\sigma_{\phi} = 0.3$ cm. The stand-alone pseudorange error standard deviation is dominated by ionospheric error and set conservatively in this analysis at $\sigma_{\rho} = 10$ m.

From solving Eq. (27), we obtain the weighted least squares solution $\delta\hat{r}$ and also the associated covariance of the position error estimate $\Sigma_{\delta\hat{r}}$ at any time epoch k. A comparable MDE for each given time relative to t_{OE} is then derived by inserting the maximum eigenvalue of the covariance matrix into Eq. (24).

Figure 11 shows the MDE traces for all satellites from a full constellation at a Chicago O'Hare GBAS ground facility site. For

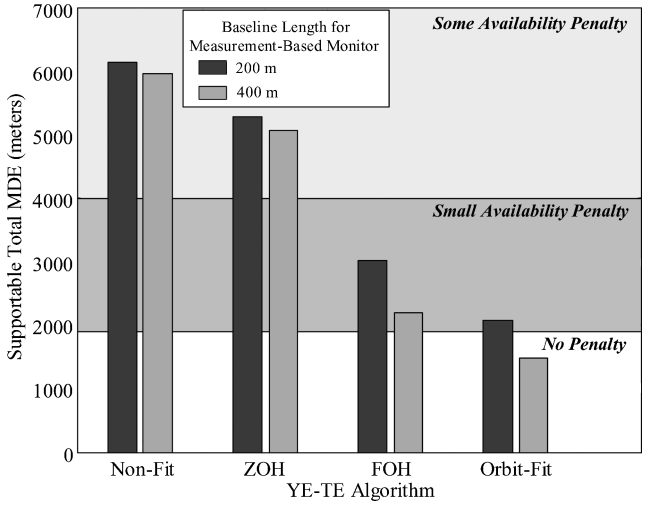

Fig. 12 Total MDE values of different YE–TE monitors combined with measurement-based monitor for various baseline lengths (200 and 400 m).

each satellite, t is arbitrarily set to zero in Fig. 11 at that given satellite's rise time. The magnitude of the MDE is directly related to the length of the pass; whereas satellites with short passes form the worst-case (upper) curves, satellites that are visible during two different time segments on the same day (connected by straight lines in Fig. 11) have lower MDE values. The MDE depends on the geometric diversity; it is dramatically improved as the baseline length is increased. The results show the worst MDE of 950 m for baseline lengths of 400 m (circled lines), 1743 m for 200 m (not shown), and 3137 m with a baseline of 100 m (dotted lines). Overall, the results demonstrate that there would be no impact on availability for baseline lengths as short as 200 m. (Recall that the desired MDE value for zero loss is 1900 m.)

VI. Total MDE and Monitor Capability

To support the YE–TE monitor assumption that the prior days' ephemerides are fault free, the measurement-based monitor described in Sec. V can be implemented to postprocess data every day. In this case, the approximate total MDE was computed using Eq. (29) by combining the $\mathrm{MDE}_{\mathrm{meas}}$ from the measurement-based monitor (taking maximum values from Fig. 11) with the $\mathrm{MDE}_{\mathrm{YETE}}$ derived for the different YE–TE monitors in Sec. IV,

$$\mathrm{MDE} \approx \sqrt{\alpha \times \mathrm{MDE}_{\mathrm{meas}}^2 + \mathrm{MDE}_{\mathrm{YETE}}^2} \tag{29}$$

The coefficient α on $\mathrm{MDE}_{\mathrm{meas}}$ varies depending on the number of prior days' ephemeris data that must be validated using the measurement-based technique: Here, $\alpha = 2$ for the parameter-based FOH monitor, and $\alpha = 1$ for all other monitors (nonfit, parameter-based ZOH, and orbit-fitting monitors). The $\mathrm{MDE}_{\mathrm{YETE}}$ term accounts for the independent error associated with the orbit projection of fault-free prior ephemerides.

The achievable total ephemeris MDEs demonstrated thus far for the YE–TE test variants discussed earlier, as well as their qualitative impact on user availability, are shown in Fig. 12. Each YE–TE monitor combined with the measurement-based monitor was validated for two cases: one with a baseline length of 200 m and the other one with a 400-m baseline. The nonfit YE–TE monitor explained in Sec. IV.A and the parameter-based ZOH YE–TE method demonstrated in Sec. IV.B support an MDE larger than 5000 m, which causes some availability penalty. An MDE of 2000–3000 m can be achieved by the parameter-based FOH YE–TE variations described in Sec. IV.B. This implies only a small loss of category 1 user availability. The orbit-fitting method of Sec. IV.C produces an MDE of 2085 m when supported by the measurement-based monitor with the 200-m baseline. This also indicates a minimal impact on availability. However, with the 400-m baseline, this method provides MDEs (1488 m) small enough to cause no loss of category 1 availability for almost all GBAS-equipped airports. Its primary disadvantage is software complexity. Implementing the orbit fitting YE–TE monitor in a GBAS ground facility would significantly complicate the software and add to its processing load. Therefore, if the limited availability penalty is deemed acceptable, it may be preferable to use the simpler parameter-based YE–TE methods in category 1 GBAS systems. These results should be valuable to select judiciously the most desirable ephemeris monitor for a specific implementation by trading off system cost and performance.

VII. Conclusions

This paper has defined type A1 (announced maneuver), type A2 (unintentional maneuver), and type B (erroneous data) threat models for satellite ephemeris errors large enough to threaten GBAS users and has derived ephemeris protection levels that connect the magnitude of potential ephemeris errors to the impact on user position. These protection levels will be required in future GBAS standards. GBAS ephemeris monitoring supports an MDE bound on the size of type A1 and B errors that may not be detected with the required missed-detection probability. (Type A2 errors are considered to be extremely improbable.) More-effective monitoring translates into lower MDEs and P values, which leads to lower ephemeris protection levels (VPL_e) and a lesser impact on GBAS user availability.

To detect type B ephemeris failures, satellite-position-based and orbit-parameter-based YE–TE tests have been proposed. The simpler nonorbit-fitting position-based method is sufficient to limit, but not eliminate, category 1 availability loss due to the addition of VPL_e. The FOH parameter-based method shows promise, using simple propagation models, to achieve lower MDEs than the nonfit position-based and ZOH parameter-based approaches. Because the availability impact of the FOH method is minimal, an attractive tradeoff exists between MDE performance and projection-model complexity. The orbit-fitting YE–TE variant reduces the ephemeris MDE enough practically to eliminate this availability loss, but this method would be complex and expensive to implement in a real-time GBAS ground station.

Measurement-based approaches have been investigated to detect type A1 ephemeris anomalies and after scheduled SV maneuvers. This method uses stand-alone pseudorange and differential carrier phase measurements across GBAS reference receiver baselines. The achievable MDE, validated by means of covariance analysis, is a strong function of baseline length, and it is shown that baseline lengths as short as 200 m are sufficient to remove availability penalty. The relevance of the measurement-based monitor to initialize the YE–TE monitor is also discussed. In this case, a baseline length of 400 m or longer may be needed depending on the desired total MDE performance and YE–TE variants.

Acknowledgments

Funding support from the Federal Aviation Administration (FAA) Local Area Augmentation System Program Office (AND-710) is appreciated. The authors would like to thank Todd Walter and Gang Xie for their help during this research. This work was also supported by the efforts of Barbara Clark of FAA AIR-130; Thomas Hsiao, Curtis Shively, Christopher Varner, and Ronald Braff of MITRE Corporation; Victor Wullschleger and John Warburton of FAA ACT-360; and others participating in RTCA SC-159 WG-4 requirements development. The advice and interest of many other people in the Stanford global positioning system research group is also appreciated.

References

[1]Braff, R., "Description of the FAA's Local Area Augmentation System (LAAS)," *Navigation*, Vol. 44, No. 4, 1998, pp. 411–423.

[2]Jefferson, D., and Bar-Sever, Y., "Accuracy and Consistency of Broadcast GPS Ephemeris Data," *Proceedings of the Institute of Navigation GPS 2000*, Inst. of Navigation, Alexandria, VA, 2000, pp. 391–395.

[3]Matsumoto, S., Pullen, S., Rotkowitz, M., and Pervan, B., "GPS Ephemeris Verification for Local Area Augmentation System (LAAS) Ground Stations," *Proceedings of the 12th International Technical Meeting*

of the Satellite Division of the Institute of Navigation, Inst. of Navigation, Alexandria, VA, 1999, pp. 691–703.

[4]Rivers, M., "2 SOPS Anomaly Resolution on an Aging Constellation," *Proceedings of the Institute of Navigation GPS 2000*, Inst. of Navigation, Alexandria, VA, 2000, pp. 2547–2550.

[5]Pullen, S., "Minutes of 2SOPS/FAA Interoperability Meeting," ARINC, Inc., Colorado Springs, CO, Feb. 1999.

[6]Spilker, J. J., "GPS Navigation Data," *Global Positioning System: Theory and Applications*, edited by B. W. Parkinson and J. J. Spilker, Vol. 1, Progress in Astronautics and Aeronautics, AIAA, Washington, DC, 1996, pp. 121–176.

[7]"Minimum Operational Performance Standards for GPS/Local Area Augmentation System Airborne Equipment," RTCA, Rept. SC-159 WG-4A, DO-253A, Washington, DC, Nov. 2001.

[8]Xie, G., Pullen, S., Luo, M., Normark, P., Akos, D., Lee, J., and Enge, P., "Integrity Design and Updated Test Results for the Stanford LAAS Integrity Monitor Testbed," *Proceedings of the Institute of Navigation 57th Annual Meeting*, Inst. of Navigation, Alexandria, VA, 2001, pp. 681–693.

[9]Pervan, B., and Chan, F. C., "Detecting Global Positioning Satellite Orbit Errors Using Short-Baseline Carrier-Phase Measurements," *Journal of Guidance, Control, and Dynamics*, Vol. 26, No. 1, 2003, pp. 122–131.

[10]Pervan, B., and Gratton, L., "Orbit Ephemeris Monitors for Local Area Differential GPS," *IEEE Transactions on Aerospace and Electronic Systems*, Vol. 41, No. 2, 2005, pp. 449–459.

[11]Enge, P., "Local Area Augmentation of GPS for the Precision Approach of Aircraft,"*Proceedings of the IEEE*, Vol. 87, No. 1, 1999, pp. 111–132.

[12]Pullen, S., Walter, T., and Enge, P., "System Overview, Recent Developments, and Future Outlook for WAAS and LAAS," *Proceedings of the Tokyo University of Mercantile Marine GPS Symposium*, Tokyo Univ., Tokyo, 2002, pp. 45–56.

[13]"Specification: Performance Type One Local Area Augmentation System Ground Facility," U.S. Federal Aviation Administration, FAA-E-2937A, Washington, DC, April 2002.

[14]"Specification: Category I Local Area Augmentation System Non-Federal Ground Facility," U.S. Federal Aviation Administration, FAA/AND710-2937, Washington, DC, May 2001.

[15]"Minimum Aviation System Performance Standards for the Local Area Augmentation System (LAAS)," RTCA, Rept. SC-159 WG-4A, DO-245, Washington DC, Sept. 1998.

[16]Hsiao, T., Shively, C., and Varner, C., "LAAS Ephemeris Error Protection Requirements & Availability," MITRE Corp./Center for Advanced Aviation System Development, Draft Rev. 1, McLean, VA, Feb. 2001.

[17]Shively, C., "Integrity from Ephemeris Test and Protection Level," MITRE Corp./Center for Advanced Aviation System Development, Draft Manuscript, McLean, VA, March 2001.

[18]Pullen, S., "False-Rejection Probability Requirements for Initial GPS Satellite Acquisition," Dept. of Aeronautics and Astronautics, Stanford Univ., Draft Ver. 1.1, Stanford, CA, May 2001.

[19]"Navstar GPS Space Segment/Navigation User Interfaces," ARINC Engineering Services, LLC, Rept. GPS-ICD-200D, El Segundo, CA, Dec. 2004.

[20]Martin, T., "MicroCosm® System Description," *MicroCosm® Software Documentation*, Vol. 1, Van Martin Systems, Inc., Rockville, MD, Sept. 1999.

[21]"GPS Enhanced Orbit Determination (GEODE) System Description and User's Guide Version 5.0," NASA Goddard Space Flight Center, CSC-96-968-04R0UD1, Greenbelt, MD, Aug. 2000.

[22]"GPS Enhanced Orbit Determination (GEODE) Mathematical Specifications Version 5.0," NASA Goddard Space Flight Center, CSC-5506-06R0UD0, Greenbelt, MD, March 2001.

[23]Gratton, L., Khanafseh, S., Pervan, B., Pullen, S., and Warburton, J., "Experimental Observations and Integrity Monitor Applications of LAAS IMLA Carrier Phase Measurements," *Proceedings of the 17th International Technical Meeting of the Satellite Division of the Institute of Navigation*, Inst. of Navigation, Alexandria, VA, 2004, pp. 2259–2270.